High-field magnetization of magnetic graphite intercalation compounds

J. T. Nicholls
Department of Physics, Massachusetts Institute of Technology, Cambridge, Massachusetts 02139

E. J. McNiff, Jr. and G. Dresselhaus
Francis Bitter National Magnet Laboratory, Massachusetts Institute of Technology, Cambridge, Massachusetts 02139
(Received 6 April 1990)

We report low-temperature, high-field ($T \leq 4.2$ K, $H = 0 - 18$ teslas) magnetization measurements of $CoCl_2$- and $NiCl_2$-graphite intercalation compounds (GIC's), both parallel ($M_\parallel$) and perpendicular ($M_\perp$) to the c axis. From the saturation magnetization values of the stage-1 and stage-2 $CoCl_2$-GIC's, we have been able to measure the anisotropy of the g values, and thus calculate the amount of XY spin anisotropy in these compounds. Magnetization measurements show that upon intercalation, the Co^{2+} ions retain their anisotropic magnetic behavior. In addition, the stage-1 $CoCl_2$-GIC's exhibit unusual hysteresis phenomena when the magnetization is measured along the c axis. Upon doping of the stage-1 $CoCl_2$-GIC's with nonmagnetic Mg^{2+} ions, the magnitude of the hysteresis in $M_\parallel(H)$ decreases and the magnetization saturates. In contrast to the behavior of the stage-1 $CoCl_2$-GIC's, stage-1 $NiCl_2$-GIC's exhibit a very small XY spin anisotropy. The magnetization $M_\parallel(H)$ is featureless for magnetic fields $H > 1$ tesla and exhibits no high-field hysteresis. The high-field c-axis magnetization of unintercalated highly oriented pyrolytic graphite was also examined; the susceptibility was $\chi \equiv M/H = -28.5 \times 10^{-6}$ emu/g, and low-field de Haas–van Alphen oscillations were observed with a frequency consistent with previously identified majority hole carriers.

I. INTRODUCTION

In this paper we present high-field magnetization measurements of several magnetic graphite intercalation compounds (GIC's). The purpose of the high-field investigation of the $CoCl_2$-GIC's is twofold. First, the spin anisotropy J_A/J can be determined from high-field magnetization measurements. Second, recent c-axis magnetization results[1] for stage-1 $CoCl_2$-GIC's exhibit unusual hysteresis effects; we have independently investigated and confirmed these effects. The purpose of the high-field investigation of the recently synthesized stage-1 $NiCl_2$-GIC's is to determine whether they exhibit similar hysteresis behavior. We also report similar high-field magnetization measurements on the newly synthesized stage-1 $Co_xMg_{1-x}Cl_2$-GIC's, again looking for the dependence of the unusual hysteresis phenomenon on the Mg concentration. Also of interest is the search of this hysteresis phenomenon and the spin anisotropy in stage-2 $CoCl_2$-GIC's.

Pristine $CoCl_2$ and $NiCl_2$ both exhibit the $CdCl_2$ crystal structure with a D_{3d}^5 ($R\bar{3}m$) space group, the point group at the magnetic cation site being D_{3d}. The energy levels of the isolated Co^{2+} ion (d^7 in a $^4F_{9/2}$ configuration) and Ni^{2+} ion (d^8 in a $^3F_4$ configuration) are states of angular momentum $L = 3$. In a cubic environment (O_h point-group symmetry), these $L = 3$ states split into $A_2 + T_1 + T_2$ levels. For the Co^{2+} ion, the twelve levels designated by $^4T_1$ comprise the ground-state multiplet, see Fig. 1, and Lines[2] has calculated the splittings within this multiplet due to the spin-orbit interaction and the trigonal crystal field (D_{3d} symmetry), where all the resulting states are doublets. Therefore, the ground-state energy is twofold degenerate with an effective spin $S = \frac{1}{2}$. The magnetic Hamiltonian for pristine $CoCl_2$ has been written by Lines[2] as

$$\mathcal{H}_{CoCl_2} = -J\sum_{i>j}\mathbf{S}_i\cdot\mathbf{S}_j + J_A\sum_{i>j}S_{iz}S_{jz} + J'\sum_{i>k}\mathbf{S}_i\cdot\mathbf{S}_k - J'_A\sum_{i>k}S_{iz}S_{kz}, \quad (1)$$

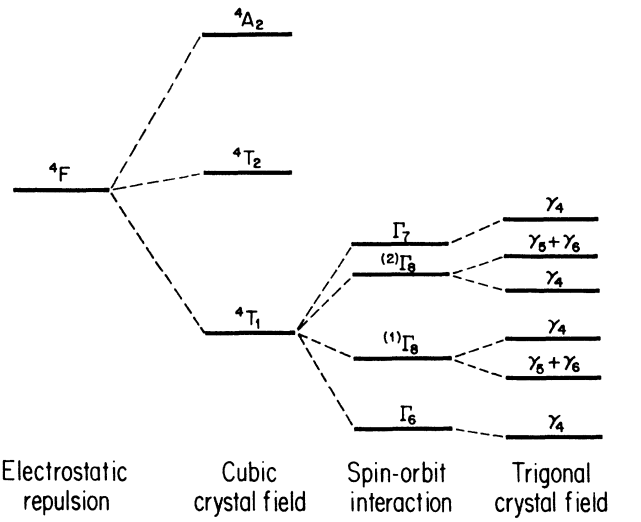

FIG. 1. Crystal-field splitting of the energy levels of the Co^{2+} ion. The cubic crystal field provides the largest interaction; further splittings are due to the spin-orbit interaction and the trigonal crystal field.

 ©1990 The American Physical Society

where the values for the intraplanar ($J = 28.5$ K, $J_A = 16.0$ K) and the interplanar ($J' = 2.1$ K, $J'_A = 3.3$ K) exchange interactions of pristine $CoCl_2$ have been measured by inelastic neutron scattering.[3] The low-temperature spin structure of $CoCl_2$ consists of ferromagnetically aligned sheets of spins that are stacked in an antiferromagnetic arrangement along the c axis.[3]

The form of the Hamiltonian [Eq. (1)] and the low-temperature spin structure of $CoCl_2$ are also appropriate for the $CoCl_2$-GIC's. Using ac magnetic susceptibility measurements, the low-field properties of the $CoCl_2$-GIC's have been investigated[4] to obtain a measure of the relative importance of the sixfold anisotropy field H_6 [not included in Eq. (1)] and the antiferromagnetic interlayer coupling J'. It was found[4] that J' is reduced by a factor of ~ 85 from its value in pristine $CoCl_2$ for the stage-1 $CoCl_2$-GIC's, and by ~ 700 in the stage-2 $CoCl_2$-GIC's. From these measurements, it is estimated that the interlayer-to-intralayer coupling ratio is $|J'/J| \sim 10^{-3}$ and $|J'/J| \sim 10^{-4}$ for the stage-1 and stage-2 $CoCl_2$-GIC's, respectively. No field-induced transition was observed[4] that could be ascribed to the presence of H_6. In this paper we investigate the properties of $CoCl_2$-GIC's when subjected to magnetic fields that are many orders of magnitude larger than J'. On the basis of Lines's theory, we use our high-field magnetization results to determine $g_\perp$ ($\mathbf{H} \perp \mathbf{c}$) and $g_\parallel$ ($\mathbf{H} \parallel \mathbf{c}$), and thus estimate J_A/J for the $CoCl_2$-GIC's (as outlined in the next paragraph). This paper, together with Ref. 4, determine the relative magnitudes of all the exchange parameters in the Hamiltonian [Eq. (1)] of the $CoCl_2$-GIC's.

In pristine $CoCl_2$, each Co^{2+} ion is surrounded by a distorted octahedron of Cl^- ions, where the trigonal warping parameter δ is a measure of the distortion (squashing) of the octahedra along the hexagonal c direction. A crystal-field theory developed by Lines[2] has related δ and the spin-orbit coupling constant λ to the difference in the g values, $g_\perp - g_\parallel$. Lines's theory,[2] based on the energy levels in Fig. 1, also gives an analytic relation between the difference in the g values of the Co^{2+} ion, $g_\perp - g_\parallel$, and the spin anisotropy ratio J_A/J; this is the solid line plotted in Fig. 2. As the difference in the g values becomes smaller, J_A/J decreases, and the Hamiltonian in Eq. (1) becomes more isotropic. Lines's theory has successfully explained the variation of $g_\perp - g_\parallel$ in the cobalt halides CoX_2, where it is found that as the halide ion X^- becomes larger, the value of δ decreases, and the spin system becomes less anisotropic.[5]

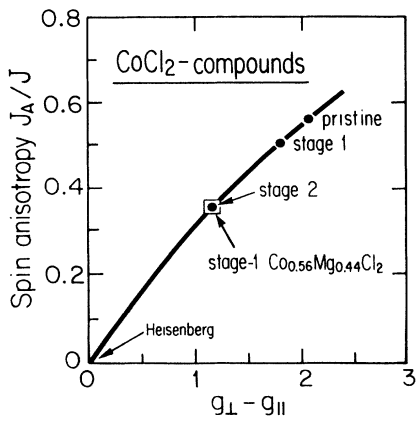

FIG. 2. The variation of the spin anisotropy (J_A/J) as a function (Ref. 2) of the difference of the g values ($g_\perp - g_\parallel$) for the Co^{2+} ion, with crystal field splittings as shown in Fig. 1. The experimentally determined values of J_A/J are shown for various $CoCl_2$ compounds.

For the case of the Ni^{2+} ion in a cubic crystal field, the parameter that characterizes the splitting of the $L = 3$ states is opposite in sign to that of the Co^{2+} ion in $CoCl_2$. Therefore, the lowest energy level for the Ni^{2+} ion in $NiCl_2$ is the $^3A_2$ state, while the threefold degenerate $^3T_1$ and $^3T_2$ states lie much higher in energy. Since the orbital angular momentum for the $^3A_2$ state is fully quenched, there is no additional splitting introduced by the spin-orbit interaction. The ground state $^3A_2$ for $NiCl_2$ is threefold spin degenerate and this suggests that $NiCl_2$ should be described by a $S = 1$ Heisenberg model. The $NiCl_2$ compounds are described by the magnetic Hamiltonian[6]

$$\mathcal{H}_{NiCl_2} = -2J \sum_{i>j} \mathbf{S}_i \cdot \mathbf{S}_j - 2J' \sum_{i>k} \mathbf{S}_i \cdot \mathbf{S}_k + D \sum_i (S_{iz}^2 - S_{ix}^2 - S_{iy}^2), \quad (2)$$

where values for the in-plane ($J = 21.7$ K), the interplanar ($J' = 0.77$ K) exchange couplings, and the single ion anisotropy term ($D = 0.4$ K) have been experimentally determined[6] for pristine $NiCl_2$. In the $NiCl_2$-GIC's, the small anisotropy in the g values ($\sim 2\%$) is more easily detected with electron-spin-resonance (ESR) measurements[7,8] rather than high-field magnetization measurements. Despite the small XY anisotropy present in the $NiCl_2$ compounds, they nevertheless exhibit magnetic XY behavior similar to the $CoCl_2$ compounds.[9]

In summary, the XY anisotropy in the magnetic Hamiltonian of the $CoCl_2$ compounds is large and is caused by the splitting of the electronic energy levels of the Co^{2+} ion by the crystal field. In contrast to the $CoCl_2$ compounds, the XY spin anisotropy in the $NiCl_2$ compounds is small and is probably due to dipolar interactions.[6]

We describe the measured GIC samples in Sec. II and some experimental details of the magnetization setup in Sec. III. In Sec. IV we present high-field magnetization data for unintercalated highly oriented pyrolytic graphite (HOPG), stage-1 $CoCl_2$-GIC's, stage-2 $CoCl_2$-GIC's, stage-1 $NiCl_2$-GIC's, stage-1 $Co_xMg_{1-x}Cl_2$-GIC's, and pristine $CoCl_2$ powder. Most of the magnetization data was measured with the applied magnetic field both parallel ($M_\parallel$) and perpendicular ($M_\perp$) to the c axis. The magnetization results are interpreted in Sec. V, and are used to estimate the magnitude of the XY spin anisotropy in the various $CoCl_2$ compounds.

II. SAMPLE PREPARATION AND CHARACTERIZATION

The stage-1 $CoCl_2$-GIC's used in our magnetization measurements were synthesized from HOPG and kish graphite. In an attempt to reproduce the unusual hysteresis behavior observed by Chouteau *et al.*,[1] the intercalation reaction was carried out for two months using high Cl_2 pressures (2–3 atm at room temperature). The intercalation temperature used was 660°C. Using (00ℓ) x-ray diffraction, the c-axis repeat distance was measured to be $I_c = 9.38 \pm 0.02$ Å. A typical intercalated sample used for magnetization measurements weighed 5 mg. The in-plane filling factors of the samples were determined from weight uptake measurements to be $\sim$ 85%. The kish-based stage-2 $CoCl_2$-GIC samples were prepared at much lower Cl_2 pressures ($\sim$ 600 Torr), and they were intercalated for one month at 560°C. The c-axis repeat distance was determined to be $I_c = 12.70 \pm 0.04$ Å. Previous investigations of stage-2 compounds made under similar conditions reported a filling factor of $\sim$75%.

From the intensities of the (00ℓ) x-ray Bragg peaks of $CoCl_2$-GIC samples based on single-crystal graphite flakes, Speck *et al.*[10] have measured the distance in the c direction z(Co-Cl) between a Co^{2+} layer and an adjacent Cl^- layer to be 1.388 ± 0.009 Å and 1.426 ± 0.051 Å for the stage-1 and stage-2 compounds, respectively. For pristine $CoCl_2$, the same distance was measured[11] to be 1.346 ± 0.012 Å. Therefore, on going from the pristine compound to stage-1 and stage-2 $CoCl_2$-GIC's there is a steady increase of z(Co-Cl); these results show that the chlorine octahedra exhibit a steady relaxation back to their perfect octahedral sites at z(Co-Cl)$= a/\sqrt{6} =$ 1.46 Å, where $a = 3.58$ Å is the Co^{2+}-Co^{2+} nearest-neighbor distance.

The stage-1 HOPG-based $NiCl_2$-GIC sample was prepared as described elsewhere,[12,13] and the (00ℓ) x-ray diffraction scan of the sample is shown in Ref. 13. The sample was cut from a larger mixed-phase sample, and so it was not possible to measure the weight uptake and to calculate a filling factor. We have assumed a filling factor of 70% for the stage-1 $NiCl_2$-GIC sample.

The stage-1 $Co_xMg_{1-x}Cl_2$-GIC's were prepared as described in Ref. 14. These samples were synthesized at high temperatures and high Cl_2 pressures, and from weight uptake measurements, the filling factors were found to be $\sim$ 85%. The Co^{2+} ion concentrations x were determined by electron microprobe measurements.[14]

III. VIBRATING SAMPLE MAGNETOMETER

The magnetization curves were obtained using a vibrating-sample magnetometer (VSM) that was specially designed and constructed by Professor Y. Shapira, Dr. S. Foner, and Dr. E. McNiff to operate in the noisy environment of the high-field Bitter magnets at the Francis Bitter National Magnet Laboratory. The magnetometer operates[15,16] by detecting the magnetic dipole field of the sample oscillating at 73.3 Hz in a uniform magnetic field, and this instrument is ideal for measuring magnetic anisotropies and magnetic saturation moments.

Each of the GIC samples was attached to the end of a glass rod that vibrates the sample vertically between the detection coils, parallel to the applied field. The attachment to the glass rod was made using Duco cement. Due to the flaky nature of the GIC samples, the walls of the magnetometer chamber were protected from possible contamination by either wrapping the sample in mylar tape, or by gluing the sample inside a protective Delrin or Teflon cup. In the configuration $\mathbf{H} \parallel \mathbf{c}$, the $CoCl_2$-GIC samples experienced very strong torque effects that sometimes gave rise to irreproducible data. The torques were large enough that, even though the sample was firmly attached by one of its c faces, it would occasionally cleave at a layer in the middle of the sample. A fully enclosed Delrin sample holder was subsequently designed to keep the sample in a fixed position with an inert fluid [Fluorinert made by 3M (St. Paul, MN)] that freezes at low temperatures.

The VSM was calibrated using a nickel sample with a saturation magnetization moment of 0.545 emu. When the GIC samples were aligned with their c axes parallel to the applied field, the accuracy of the magnetization data was well within $\pm 5.0\%$ of the signal. In the other sample configuration, $\mathbf{H} \perp \mathbf{c}$, the sample occupies a greater length of the detection coils and there is a breakdown of the dipole approximation. The accuracy of the magnetometer was thus reduced for measurements in this configuration. The greatest source of error in all the quoted results came from the samples themselves, principally from inaccuracies in the weight uptake measurements. Additional errors were sometimes introduced when small flakes of the sample were lost in the Duco cement while the sample was demounted and switched from one configuration to the other.

IV. HIGH-FIELD MAGNETIZATION RESULTS

In this section high-field magnetization results are presented for all the samples that were investigated. Most of the experimental data shown in the figures were obtained at 4.2 K. It was found that on cooling to 1.3 K the general features of the magnetization curves did not change. For comparison with the magnetization results of other groups,[1,17,18] all magnetizations are quoted in units of emu/(g of GIC). Ideally, the data should be quoted in emu per mole of magnetic ion; this latter convention has been adopted for comparison of the susceptibilities.

A. Pure graphite

To check the sensitivity of the magnetometer, the magnetization $M_{\parallel}(H)$ of pristine HOPG was measured with the magnetic field $\mathbf{H}$ aligned parallel to the sample c axis. The results for $M_{\parallel}(H)$ at $T = 4.2$ K are shown in Fig. 3(a), and are in good agreement with the previously published results of Chouteau and Briggs.[19] The HOPG has a diamagnetic dc susceptibility of $\chi^{dc} \equiv M/H =$

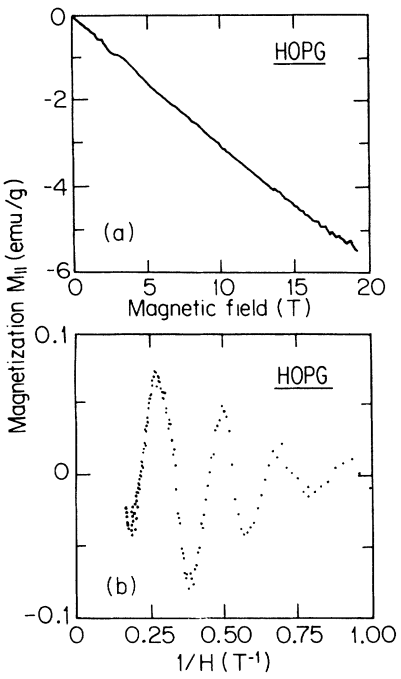

FIG. 3. (a) The c-axis magnetization $M_{||}(H)$ of HOPG at $T = 4.2$ K. (b) The low-field (≤ 3 teslas) dHvA oscillations are plotted vs $1/H$.

-28.5×10^{-6} emu/g. The deviations of $M_{||}(H)$ from linear behavior at low fields, $H < 3$ teslas, are due to de Haas–van Alphen (dHvA) oscillations. These oscillations are more clearly seen by subtracting the dc susceptibility from the raw data, and the dHvA oscillations are plotted versus $1/H$ in Fig. 3(b). The oscillations have a frequency of $\nu_{\mathrm{dHvA}} \approx 4.8$ teslas, and of the various possible Fermi surface oscillations (as designated in Ref. 20) we identify this frequency to be due to the majority hole carriers. The sensitive measurements reveal a slight upward curvature in the magnetization, as predicted by theory.[21] The fluctuations in the high-field ($H > 13$ teslas) magnetization were due to magnet noise caused, for example, by current arcing between the copper plates of the Bitter magnet.

B. Stage-1 $CoCl_2$-GIC's

The magnetization curves for a stage-1 $CoCl_2$-GIC sample at 4.2 K are shown in Fig. 4. The virgin magnetization curve, labeled (a), was obtained by placing the sample in the magnetometer, and, without maximizing the signal, a field sweep was executed. The signal $M_{||}(H)$ shows three approximately linear regions: (1) a sharp increase at low fields of about 0.28 emu/mol, (2) a weaker rise of 0.075 emu/mol in the intermediate field region 1-12 teslas, (3) an even weaker slope of 0.018 emu/mol at the highest fields. These susceptibilities are denoted by $\chi_{||}^{(1)}$, $\chi_{||}^{(2)}$, and $\chi_{||}^{(3)}$, respectively. On reducing the magnetic field, the magnetization curve, labeled

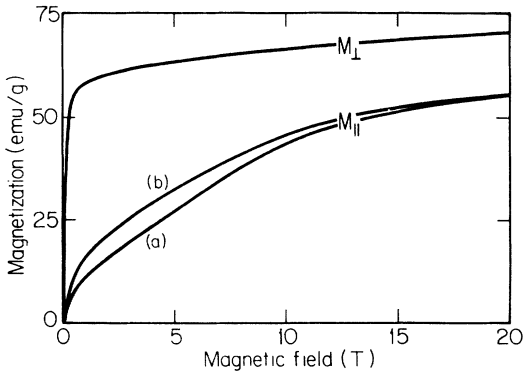

FIG. 4. Magnetization of stage-1 $CoCl_2$-GIC at 4.2 K. The virgin trace in $M_{||}(H)$ is labeled (a), and on reducing the applied magnetic field, curve (b) was obtained. The magnetization for the configuration $\mathbf{H} \perp \mathbf{c}$, labeled $M_\perp$, is also shown.

(b), was obtained; these data show considerable hysteresis over the whole field range. Successive up and down sweeps (2 teslas/min) of the field show decreasing hysteresis. Upon thermal annealing of the sample at room temperature for 5 min, we could not recover curve (a). Furthermore, we could not recover curve (a) even when the sample was allowed to anneal at room temperature for two weeks. The down and up field sweeps in a negative field (see Fig. 5) show smaller hysteresis than the earlier up and down sweeps in a positive field. The diminishing of the observed hysteresis with successive sweep cycles was observed to be independent of whether the sign of the magnetic field was positive or negative. Referring to Fig. 5, it appears that with enough field sweeps, the c-axis magnetization will become antisymmetric, that is, $M_{||}(-H) = -M_{||}(H)$. This implies that there is no remanent magnetization, though this could not be explicitly checked due to the large remanent fields of the Bitter magnets. In the configuration, $\mathbf{H} \perp \mathbf{c}$, the magne-

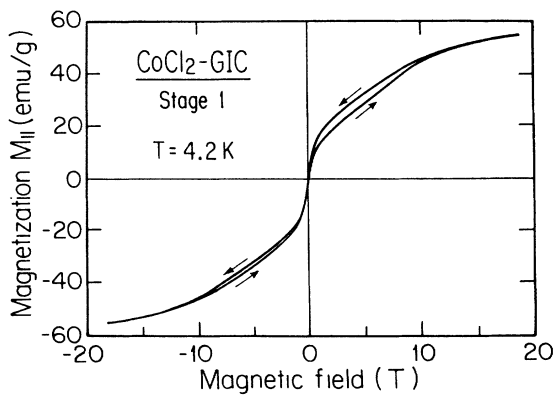

FIG. 5. A full $M_{||}(H)$ hysteresis loop for a stage-1 $CoCl_2$-GIC sample at 4.2 K. The field was swept in the sequence 0 tesla → 18 teslas → 0 tesla → −18 teslas → 0 tesla, and this figure shows clearly that there is no remanent magnetization.

tization curve $M_\perp$ saturates quickly and has a high-field susceptibility of 0.011 emu/mol, and shows no hysteresis.

C. Stage-2 $CoCl_2$-GIC's

The magnetization curves for a stage-2 $CoCl_2$-GIC sample at 4.2 K are shown in Fig. 6. In the parallel configuration, $M_\parallel$ rises quickly below 1 tesla, and then increases linearly at a rate of 0.042 emu/mol. At even higher field values, two contributions to the magnetization were observed: a linear contribution of 0.014 emu/mol and also dHvA oscillations due to the graphitic hole carriers. The dHvA oscillations indicate that the samples are of good quality ($\omega_c\tau \gg 1$, where $\omega_c = eB/m^*c$, τ is the relaxation time, and m^* is the effective mass of the hole carrier). These oscillations have been separated out and plotted versus $1/H$ (see figure inset) to display more clearly the periodicity of the oscillations which were found to have a frequency of $\nu_{\mathrm{dHvA}} = 150$ teslas. Since the main focus of the present work is on the hysteresis and anisotropy of the high-field magnetization, these dHvA oscillations were not studied in detail. The magnetization data for the stage-2 sample (see Fig. 6) show no hysteresis or remanence, in contrast to the stage-1 $M_\parallel(H)$ data. For the stage-2 $CoCl_2$-GIC sample, $M_\perp$ saturates below 1 tesla and has a high-field susceptibility of 0.0067 emu/mol. The $M_\perp$ behavior is similar to its stage-1 counterpart.

D. Stage-1 $NiCl_2$-GIC's

The magnetization trace for a stage-1 $NiCl_2$-GIC sample with **H** || **c** is shown in Fig. 7. Although stage-1 $NiCl_2$-GIC's have the same structure[12] as stage-1 $CoCl_2$-GIC's there was no evidence of any hysteresis in the high-field c-axis magnetization traces. In an attempt to induce some hysteresis, the sample was introduced into the VSM in a field of 5 teslas and measurements in the sequence 5 teslas→ 0 tesla→ −5 teslas→ 0 tesla were performed at 4.2 K. The resulting data, see Fig. 7, show no hysteresis or remanent magnetization. Assuming a 70% filling factor, the observed saturation magnetization of 60 emu/g translates to a g value of $g_\parallel = 2.2$, in agreement with more accurate ESR measurements[8] which yield $g_\parallel = 2.25$. At higher magnetic fields (5 – 18 teslas), the c-axis magnetization remains constant and featureless.

A comparison of the Néel temperatures T_N and g values of stage-1 $NiCl_2$-GIC's prepared by different groups is given in Table I. The results of El Hafidi *et al.*,[22] with a lower Néel temperature, suggests that their sample has a low intercalate filling factor. Furthermore, their value for the average g-value $g_{\mathrm{av}} = 1.49$ is incompatible with the g values measured here and elsewhere.[8]

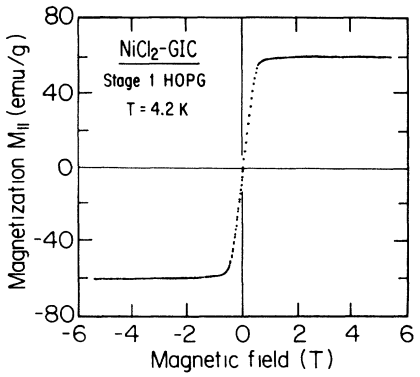

FIG. 7. The c-axis magnetization $M_\parallel(H)$ of HOPG-based stage-1 $NiCl_2$-GIC at 4.2 K. The field was swept in the sequence 5 teslas → 0 tesla → −5 teslas → 0 tesla to check for hysteresis.

E. Stage-1 $Co_xMg_{1-x}Cl_2$-GIC's

The virgin c-axis magnetization $M_\parallel$ traces for stage-1 $Co_xMg_{1-x}Cl_2$-GIC's for various Co concentrations are shown in curves a–f of Fig. 8. For Co concentrations

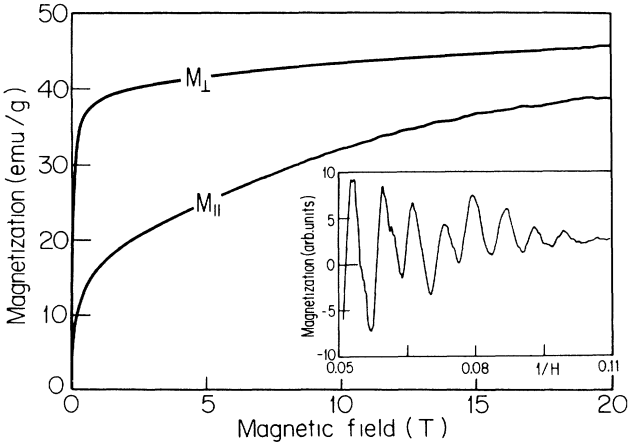

FIG. 6. Magnetization ($M_\perp$ and $M_\parallel$) of stage-2 $CoCl_2$-GIC at 4.2 K. The figure inset shows the dHvA oscillations vs $1/H$ that have been separated from the other high-field $M_\parallel(H)$ contributions.

TABLE I. Comparison of the Néel temperature T_N and g values for stage-1 $NiCl_2$-GIC's.

Property	Nicholls *et al.*	El Hafidi *et al.* (Ref. 22)	Flandrois *et al.* (Ref. 8)
T_N (K)	23 ± 0.5[a]	17.85[b]	21.0[b]
$g_\parallel$	2.2[b]		2.25[c]
$g_\perp$			2.25[c]
g_{av}		1.49[b,d]	2.25[c]

[a] From ac susceptibility measurements (Refs. 12 and 13).
[b] From magnetization measurements.
[c] From ESR measurements.
[d] Powder sample.

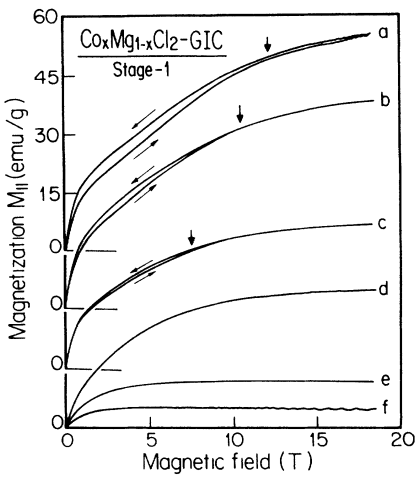

FIG. 8. The virgin c-axis magnetization $M_{||}(H)$ traces for stage-1 $Co_xMg_{1-x}Cl_2$-GIC's of Co concentration a $x = 1$, b $x = 0.92$, c $x = 0.77$, d $x = 0.56$, e $x = 0.20$, and f $x = 0.09$. The arrows (↓) show approximately where there is a high-field knee in the magnetization curve.

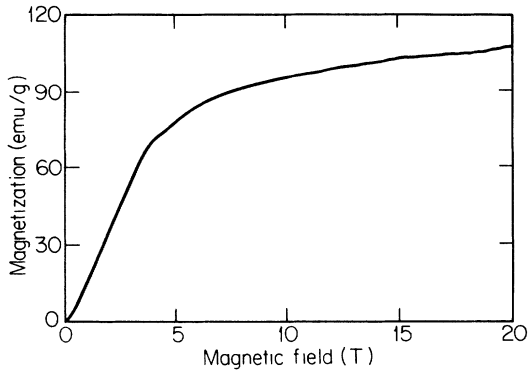

FIG. 9. Magnetization of pristine $CoCl_2$ powder at 4.2 K. No hysteresis was observed, in contradiction with the measurements of Chouteau *et al.* (Ref. 24).

greater than $x = 0.65$, the virgin $M_{||}(H)$ traces show hysteresis when the magnetic field was swept up and down, though the size of the hysteresis diminishes as the Mg concentration $(1 - x)$ increases. No hysteresis was detected in traces d, e, and f, Fig. 8. The high-field magnetization $M_{||}(H)$ saturates for the weakly doped ($x = 0.09, 0.2$) compounds, whereas $M_{||}(H)$ does not saturate for the more concentrated compounds.

As the Co concentration x decreases, the knee in the c-axis magnetization curve (shown approximately with an arrow ↓) shifts to lower field values and becomes less pronounced.

F. High-field magnetization of pristine $CoCl_2$

Insight into the magnetic properties of the $CoCl_2$-GIC's is provided by measurements on pristine $CoCl_2$. Unfortunately, the previous[23] magnetization measurement on anhydrous $CoCl_2$ was carried out in magnetic fields below 3 teslas. To gain some quick order-of-magnitude information about the Van Vleck contribution to the susceptibility (discussed in Sec. V C) of the pristine compound, we have measured the magnetization of powder $CoCl_2$ (see Fig. 9). Pristine $CoCl_2$ degrades quickly when exposed to the water vapor in the air and must be handled carefully. The low-field (< 2 teslas) linear regime agrees with the data of Starr *et al.*[23] At higher field values $H > 10$ teslas, the magnetization exhibits a linear susceptibility of 0.0112 emu/mol that corresponds to $\frac{1}{3}\chi_{||} + \frac{2}{3}\chi_{\perp}$. The claim by Chouteau *et al.*[24] that there is large hysteresis in the high-field magnetizations $M_{\perp}(H)$ and $M_{||}(H)$ of pristine single-crystal $CoCl_2$ is in disagreement with our powder measurements of $CoCl_2$ (see Fig. 9) that exhibit no hysteresis.

V. DISCUSSION

Magnetization curves for the $CoCl_2$-GIC's exhibit many different phenomena that are discussed in greater detail in this section. The spin anisotropy and hysteresis effects (the two original purposes for measuring the high-field magnetization) are discussed first, followed by less extensive discussions of the high-field susceptibility, and quantum oscillatory phenomena.

A. Spin anisotropy

The Co^{2+} spin in the $CoCl_2$-GIC's is highly anisotropic, as can be seen in the high-field portions of the $M_{\perp}$ and $M_{||}$ traces in Figs. 4 and 6. When the magnetic field is applied in the xy plane ($\mathbf{H} \perp \mathbf{c}$), the high-field magnetization curves are featureless and no hysteresis effects are observed. The $M_{\perp}(H)$ curves for stage-1 and stage-2 $CoCl_2$-GIC's look very similar; any differences between the two curves occur at low-field values ($\ll 0.1$ tesla) where there is a competition between the applied field $\mathbf{H}$ and the interplanar antiferromagnetic coupling J'. In the other configuration $\mathbf{H} \parallel \mathbf{c}$, the applied magnetic field pulls the spins out of the easy xy plane. The strength of the magnetic field H_A that is required to do this is determined by the magnitude of the XY anisotropy term J_A [see Eq. (1)]; these two quantities are related approximately through the expression

$$H_A = zSJ_A/g\mu_B, \tag{3}$$

where $g \approx 6$, and $z = 6$ is the number of nearest-neighbor spins in the intercalate plane. From the value of $J_A = 16$ K in pristine $CoCl_2$, Eq. (3) predicts there to be a field-induced feature at approximately 15 teslas. Looking carefully at the trace a in Fig. 8, there is a knee in $M_{||}(H)$ at ~ 12 teslas. As the stage-1 $CoCl_2$-GIC's are doped with nonmagnetic Mg^{2+} ions, this high-field feature decreases to ~ 10 teslas (trace b, Fig. 8) and then

TABLE II. Comparison of magnetization results for stage-1 and stage-2 $CoCl_2$-GIC's, stage-1 $Co_{0.56}Mg_{0.44}Cl_2$-GIC, and powder $CoCl_2$.

	Property[a]	This work	Oguro *et al.* (Ref. 17)	Chouteau *et al.* (Ref. 1)	Wiesler *et al.* (Ref. 18)	Theory
Powder $CoCl_2$	χ_{av}	0.0112				
	$M_{av}^{sat}(\mu_B)$	2.10	-	-	-	2.10[d]
	J_A/J					0.62[d]
Stage-1 $CoCl_2$-GIC	$\chi_{\parallel}^{(1)}$	0.28				
	$\chi_{\parallel}^{(2)}$	0.075	0.049			
	$\chi_{\parallel}^{(3)}$	0.018		0.0158		
	$\chi_{\perp}$	0.011	0.0064	0.0117		
	$M_{\parallel}^{sat}(\mu_B)$	1.40		1.95	2.38[c]	1.32[d]
	$M_{\perp}^{sat}(\mu_B)$	2.30	2.63	2.7	2.97[c]	2.49[d]
	J_A/J	0.50		0.44	0.38[c]	0.62[d]
Stage-1 $Co_{0.56}Mg_{0.44}Cl_2$-GIC	$M_{\parallel}^{sat}(\mu_B)$	1.65[b]				
	$M_{\perp}^{sat}(\mu_B)$	2.23[b]				
	J_A/J	0.35				
Stage-2 $CoCl_2$-GIC	$\chi_{\parallel}$	0.014				
	$\chi_{\perp}$	0.0067	0.0039			
	$M_{\parallel}^{sat}(\mu_B)$	1.43			2.37[c]	1.32[d]
	$M_{\perp}^{sat}(\mu_B)$	2.01	2.23		3.2[c]	2.49[d]
	J_A/J	0.35			0.48[c]	0.62[d]

[a]The susceptibilities χ are quoted in units of emu/mol.
[b]From Ref. 14.
[c]Derived from high-temperature susceptibility data; all other results were obtained from high-field magnetization experiments.
[d]From Ref. 5.

moves to lower fields (trace c) and becomes smaller in intensity as the Co^{2+} ion concentration decreases. There are two reasons for these observations. First, the number of nearest in-plane magnetic neighbors is decreased through doping; hence there is a reduction of z in Eq. (3). Second, as the Mg^{2+} ion concentration increases, the Cl^- ion octahedra [as measured by increasing $I_c(x)$ as x decreases[14]] move closer to the ideal octahedral positions, reducing both the trigonal distortion δ and the spin anisotropy J_A/J.

Using the values of $M_{\perp}^{sat}$ and $M_{\parallel}^{sat}$ to obtain $g_{\perp}$ and $g_{\parallel}$, we use the theory of Lines to calculate J_A/J for the $CoCl_2$-GIC's. We find that upon intercalation, the value of J_A/J becomes smaller (see Fig. 2 and Table II), and the spin anisotropy becomes less XY-like due to a relaxation of the structure. Besides structural data,[10] further evidence for the relaxation of the Cl^- octahedra comes from measurements[25] of the reduction of the strength of the NMR transfer hyperfine field on going from pristine $CoCl_2$ to stage-1 $CoCl_2$-GIC's. The magnitude of the hyperfine field reflects the degree of interaction between the ^{35}Cl nuclear spin and the magnetic moment of the Co^{2+} ion. The more squashed the Cl^- octahedron, the stronger the hyperfine field interaction. The reduction of J_A/J upon intercalation increases as the number of graphene layers increases (see Fig. 2).

As described in a recent paper[14] on the magnetic properties of the stage-1 $Co_xMg_{1-x}Cl_2$-GIC's, there is a loss of low-temperature long-range antiferromagnetic order when the Co^{2+} ion concentration is less than the critical concentration $x_p = 0.65$. As shown in Fig. 9 of that same paper,[14] there is anisotropy in the saturation magnetization even for a stage-1 $Co_{0.56}Mg_{0.44}Cl_2$-GIC which shows no transition to an antiferromagnetic phase at low temperature. This latter observation is a clear indication that the XY spin anisotropy is determined by the local crystal environment, as described in Sec. I.

The results of $M_{\perp}(H)$ and $M_{\parallel}(H)$ for the stage-2 $CoCl_2$-GIC's (Fig. 6) agree with the results of Oguro *et al.*[17] in the 0–5 teslas field region. However, we could not reproduce the results of Wiesler *et al.*[18] whose magnetization measurements look more isotropic. Instead, we found that the magnetization components $M_{\perp}$ and $M_{\parallel}$ have saturation values close to those predicted by the theory previously applied to pristine $CoCl_2$. In Table II we have summarized our measured saturation magnetizations ($M_{\parallel}^{sat}$ and $M_{\perp}^{sat}$) and spin anisotropies (J_A/J) for the various $CoCl_2$ systems; the corresponding published results of other research groups[1,17,18] are also tabulated.

In summary, we know from structural studies that the Cl^-–Co^{2+}–Cl^- sandwich structure is preserved when $CoCl_2$ is intercalated into graphite. We have shown, using the crystal-field theory of Lines,[2] that the anisotropy of the Co^{2+} spin is preserved when the Co^{2+} ion is intercalated. It would be of interest to perform these magnetization measurements on higher stage $CoCl_2$-GIC's.

B. Hysteresis effects in stage-1 $Co_xMg_{1-x}Cl_2$-GIC's

For stage-1 $Co_xMg_{1-x}Cl_2$-GIC's with $x > 0.56$ the hysteresis effects in the virgin traces of $M_{\|}(H)$ are not recovered when the sample is annealed well above the three-dimensional magnetic ordering temperature. This is incompatible with the properties of a pure spin system. For example, spin glasses are known to have similarly long relaxation times; however, they usually exhibit a remanent magnetization. Spin glasslike effects have been observed[26] in stage-2 $CoCl_2$-GIC's; however, it is important to distinguish that these effects were observed at low fields (~100 mOe) and at low frequencies (~mHz) and involve only a small fraction of the total number of Co^{2+} spins in the sample. Our observations of hysteresis behavior for stage-1 $CoCl_2$-GIC's are similar to those of Chouteau *et al.*,[1] except that their measurements show an even larger hysteresis. We propose that upon application of a strong field, $\mathbf{H} \| \mathbf{c}$, the highly anisotropic Co^{2+} ion causes the intercalate layer to undergo a magnetostriction effect. To relieve the induced strain, the ions within the magnetic domains undergo some sort of rearrangement that reduces their anisotropy energy. The radius of gyration R_g of the domains, as measured[27] by small-angle neutron scattering at 4.2 K, was found to be invariant with respect to a high magnetic field $\mathbf{H} \| \mathbf{c}$. As expected, diffusion processes are frozen out at liquid-helium temperature. The current understanding of the meaning of R_g is not clear, since there appear to be many different length scales that are probed by different experiments. These issues are addressed elsewhere.[14,28]

Due to spin-orbit coupling, the Co^{2+} ion in $CoCl_2$ and its graphite intercalation compounds exhibits highly anisotropic magnetic behavior; for the same reason the Co^{2+} ion should also exhibit a strong magnetostriction effect. Indeed, low-field[29] and high-field[24] magnetostriction effects have been observed in pristine single-crystal $CoCl_2$. In a simple theory[29] of this effect, there is a coupling between the magnetic and mechanical degrees of freedom when the low temperature state of the system exhibits long-range antiferromagnetic order. As the Co^{2+} ion concentration is decreased, the magnetic hysteresis in the stage-1 $Co_xMg_{1-x}Cl_2$-GIC samples (see Fig. 8) first diminishes and then disappears ($x \leq 0.56$). For concentrations $x \leq 0.56$ there is no low-temperature antiferromagnetic order and no hysteresis, in agreement with the simple predictions. The hysteresis effect was not observed in $M_{\|}(H)$ traces of stage-2 $CoCl_2$-GIC samples, a possible explanation being that the extra graphene layer is a very effective absorber of the magnetic strain that is induced between the $CoCl_2$ layers. The $M_{\|}(H)$ results for a stage-1 $NiCl_2$-GIC sample (see Fig. 7) show no hysteresis, presumably because the Ni^{2+} ion exhibits almost isotropic magnetic behavior.

We should, however, state that all the unusual hysteresis behavior observed could also be explained by magnetic torque effects. That is, in spite of our efforts to keep the samples fixed in the frozen fluid, there could be some internal movement of the GIC layers that is changing the microstructure of the sample.

C. High-field susceptibility

At the highest field values, the magnetization data of the undiluted $CoCl_2$-GIC's show a term that is directly proportional to the applied field. It was originally thought[24,30] that this was a temperature-independent Van Vleck susceptibility χ_{VV}. However, from our measurements of the dilute stage-1 $CoCl_2$-GIC's, see Fig. 8, we now believe that the most likely cause for the unusually high susceptibilities $\chi_{\|}$ at high magnetic fields in the pure $CoCl_2$-GIC's is due to the incomplete alignment of the spins in the c direction. In the more dilute compounds, there is a reduction of H_A, and for high fields $H \gg H_A$ the magnetization $M_{\|}(H)$ becomes saturated.

D. Quantum oscillatory phenomena

The dHvA oscillations observed in $M_{\|}(H)$ of the stage-2 $CoCl_2$-GIC can be explained by a cylindrical Fermi surface. On reducing the temperature to 1.3 K, the oscillations did not grow dramatically; this indicates a large amount of electron scattering that gives rise to a high Dingle temperature T_D. In other stage-2 compounds ($CuCl_2$-GIC's) with electronic properties that are expected to be similar to the stage-2 $CoCl_2$-GIC's, the Dingle temperature has been measured[20] to be $\sim 10-20$ K; therefore, the term T_D will dominate in the expression $\exp[-\text{const}(T+T_D)]$ that predicts the amplitude of the quantum oscillations. As expected,[31] dHvA oscillations were not observed in the stage-1 $CoCl_2$-GIC samples.

VI. SUMMARY

In summary, high-field measurements of the magnetization $M_{\|}(H)$ and $M_{\perp}(H)$ have been made for stage-1 and stage-2 $CoCl_2$-GIC's, for stage-1 $NiCl_2$-GIC's and for the stage-1 alloy system $Co_xMg_{1-x}Cl_2$-GIC's for various x values. Particular emphasis has been given to the anisotropy of the magnetization and the search for the unusual hysteresis behavior that is observed in stage-1 $Co_xMg_{1-x}Cl_2$-GIC's for $x \geq 0.65$, showing that the hysteresis effect is suppressed by addition of Mg. Arguments are presented in support of a magnetostriction mechanism for the origin of this unusual hysteresis phenomenon. The absence of the hysteresis effect in $M_{\|}(H)$ for the stage-1 $NiCl_2$-GIC as well as the functional dependence of $M_{\|}(H)$ support a small value for the anisotropy D for this compound, consistent with the behavior of pristine $NiCl_2$. For all materials studied, the saturation magnetization was determined for both $H \| c$ axis and $H \perp c$ axis, and good agreement was obtained with previous relevant measurements, as indicated in Tables I and II.

ACKNOWLEDGMENTS

This work was supported by National Science Foundation Grant (NSF) No. DMR-88-19896. The Francis Bitter National Magnet Laboratory at the Massachusetts Institute of Technology, where the high-field magnetization measurements were performed, is supported by the National Science Foundation. We are grateful to Professor M.S. Dresselhaus for her helpful comments and encouragement, and to Professor Y. Shapira for help in the early stages of this work. HOPG was kindly supplied by Dr. A.W. Moore of Union Carbide Corporation, and kish graphite was kindly provided by Professor H. Suematsu of the University of Tokyo.

[1] G. Chouteau and R. Yazami, Europhys. Lett. **3**, 229 (1987).
[2] M. E. Lines, Phys. Rev. **131**, 546 (1963).
[3] M. T. Hutchings, J. Phys. C **6**, 3143 (1973).
[4] J. T. Nicholls and G. Dresselhaus, J. Phys. Condens. Matter (to be published).
[5] G. Mischler, D. J. Lockwood, and A. Zwick, J. Phys. C **20**, 299 (1987).
[6] P. A. Lindgard, R. J. Birgeneau, J. Als-Nielsen, and H. J. Guggenheim, J. Phys. C **8**, 1059 (1975).
[7] M. Suzuki, K. Koga, and Y. Jinzaki, J. Phys. Soc. Jpn. **53**, 2745 (1983).
[8] S. Flandrois, J. Amiell, B. Agricole, E. Stumpp, C. Ehrhardt, and P. Schubert, Synth. Met. **34**, 531 (1989).
[9] G. Dresselhaus, J. T. Nicholls, and M. S. Dresselhaus, in *Graphite Intercalation Compounds II, Springer Series in Materials Science*, edited by H. Zabel and S. A. Solin (Springer-Verlag, Berlin, 1990, in press).
[10] J. S. Speck, J. T. Nicholls, B. J. Wuensch, J. M. Delgado, M. S. Dresselhaus, and H. Miyazaki (unpublished).
[11] M. K. Wilkinson, J. W. Cable, E. O. Wollan, and W. C. Koehler, Phys. Rev. **113**, 497 (1959).
[12] J. T. Nicholls, J. S. Speck, and G. Dresselhaus, Phys. Rev. B **39**, 10 047 (1989).
[13] J. T. Nicholls and G. Dresselhaus, Synth. Met. **34**, 519 (1989).
[14] J. T. Nicholls and G. Dresselhaus, Phys. Rev. B **41**, 9744 (1990).
[15] S. Foner, Rev. Sci. Instrum. **30**, 548 (1959).
[16] S. Foner and E. J. McNiff, Jr., Rev. Sci. Instrum. **39**, 171 (1968).
[17] I. Oguro, M. Suzuki, and H. Yasuoka, Synth. Met. **12**, 449 (1985).
[18] D. G. Wiesler, M. Suzuki, P. C. Chow, and H. Zabel, Phys. Rev. B **34**, 7951 (1986).
[19] G. Chouteau and A. Briggs, Solid State Commun. **21**, 785 (1977).
[20] N. B. Brandt, S. M. Chudinov, and Y. G. Ponomarev, *Semimetals 1 Graphite and its Compounds*, Vol. 20.1 of *Modern Problems in Condensed Matter Sciences* (North-Holland, Amsterdam, 1988).
[21] N. Jacobi and J.-P. Jay-Gerin, Solid State Commun. **21**, 789 (1977).
[22] M. El Hafidi, G. Chouteau, and R. Yazami, Synth. Met. **34**, 525 (1989).
[23] C. Starr, F. Bitter, and A. R. Kaufmann, Phys. Rev. **58**, 977 (1940).
[24] G. Chouteau, in *Extended Abstracts of the 1988 Materials Research Society Symposium on Graphite Intercalation Compounds*, edited by M. Endo, M.S. Dresselhaus, and G. Dresselhaus (MRS, Pittsburgh, PA, 1988), p. 61.
[25] T. Tsuda, H. Yasuoka, and M. Suzuki, Synth. Met. **12**, 461 (1985).
[26] M. Matsuura, Y. Endoh, T. Kataoka, and Y. Murakami, J. Phys. Soc. Jpn. **56**, 2233 (1987).
[27] G. Chouteau, J. Schweizer, F. Tasset, and R. Yazami, Synth. Met. **23**, 249 (1988).
[28] J. S. Speck and M. S. Dresselhaus, Synth. Met. **34**, 211 (1989).
[29] A. F. Lozenko, P. E. Parkhomchuk, S. M. Ryabchenko, and P. A. Trotsenko, Fiz. Nizk. Temp. **14**, 941 (1988) [Sov. J. Low Temp. Phys. **14**, 517 (1988)].
[30] J. T. Nicholls, Y. Shapira, E. J. McNiff, Jr., and G. Dresselhaus, Synth. Met. **23**, 231 (1988).
[31] M. S. Dresselhaus and G. Dresselhaus, Adv. Phys. **30**, 139 (1981).